

Rotate, Clip, and Partition: Towards W2A4KV4 Quantization by Integrating Rotation and Learnable Non-uniform Quantizer

Euntae Choi*, Sumin Song*, Woosang Lim, Sungjoo Yoo

Seoul National University

euntae.choi175@gmail.com, songsm921@snu.ac.kr,

ftyg656512@snu.ac.kr, sungjoo.yoo@gmail.com

Abstract

We propose Rotate, Clip, and Partition (RCP), a Quantization-Aware Training (QAT) approach that first realizes extreme compression of LLMs with W2A4KV4(2-bit weight, 4-bit activation, and 4-bit KV-cache) configuration. RCP integrates recent rotation techniques with a novel non-uniform weight quantizer design, by quantitatively analyzing the impact of random rotation on 2-bit weight quantization. Our weight quantizer features Learnable Direct Partitioning (LDP), which introduces learnable parameters to directly learn non-uniform intervals jointly with LLM weights. We also present a specialized GPU kernel that supports GEMV on non-uniform W2A4. Experiments show that RCP can compress LLaMA-2-7B to W2A4KV4 with a loss of only 2.84 WikiText2 ppl and 5.29 times reduced memory footprint. Furthermore, RCP can quantize challenging mobile-targeted LLaMA-3.2 models and domain-specific WizardCoder-7B and MetaMath-7B with no critical problems such as convergence failure and repetition. Code will be made available at [blind_review](#).

1 Introduction

Large language models (LLMs) have made significant advancements, but their growing size and resource demands create challenges for deployment across data centers and mobile devices. To address these constraints, extensive research efforts have focused on improving the efficiency of LLM serving through various strategies. Quantization, one of the various methods, has emerged as a particularly straightforward and effective method for reducing memory consumption and inference costs without severely compromising accuracy. By lowering the numerical precision of parameters and intermediate representations, quantization leverages hardware capabilities such as half-precision and integer tensor cores.

*these authors contributed equally.

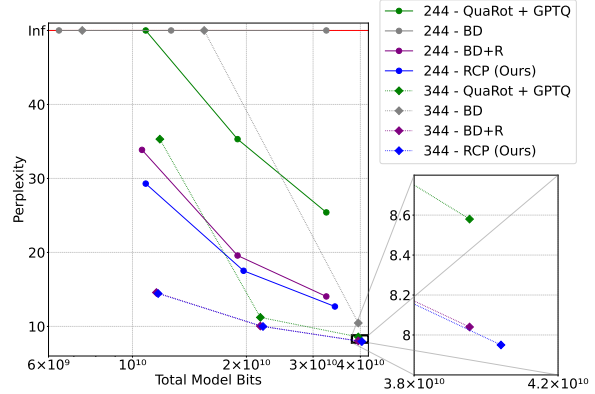


Figure 1: Bit-Level scaling laws for perplexity for LLaMA-3 (AI@Meta, 2024) (1B, 3B, 8B).

Post-Training Quantization (PTQ) is a quantization technique that performs well up to levels like W4A4¹, maintaining acceptable accuracy compared to original models. However, as the bit-width decreases, the representable information becomes insufficient, making it difficult to address challenges such as salient weights, outliers, and the quantization of activations and the KV-cache. To address these issues, rotation techniques (Ashkboos et al., 2024b; Liu et al., 2024b) have proven effective at W4A4KV4. Nevertheless, extending these methods to even lower bit widths, such as W2 or W3, remains insufficient, as the severe information bottleneck cannot be overcome with a uniform quantization and PTQ, ultimately resulting in a loss of generation quality.

In this work, we propose a Quantization-Aware Training (QAT) approach called Rotate, Clip, and Partition (RCP), which integrates rotation techniques with non-uniform quantization strategies to achieve extreme compression of LLMs, specifically realizing W2A4KV4 configurations. Our method jointly optimizes quantization parameters and model weights by systematically incorporating rotation and non-uniform group quantization. We

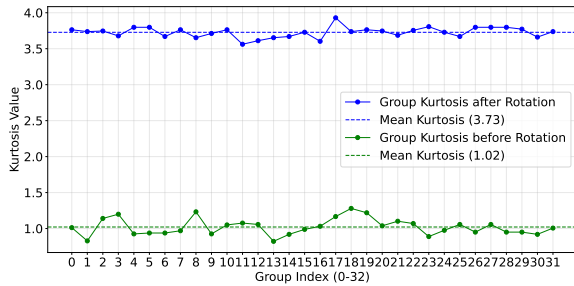
¹We call l -bit weight, m -bit activation and n -bit KV-cache $WlAmKVn$ like W2A4KV4.

for each linear layer and then uses them as initial values for learnable clipping f as follows:

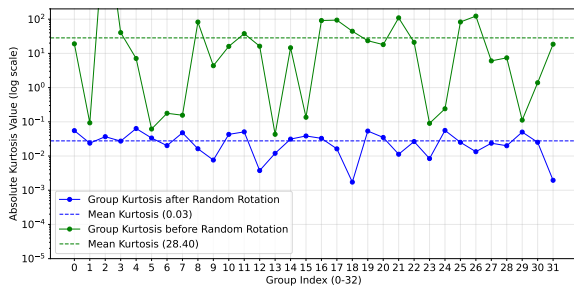
$$f(\mathbf{W}, \beta, \gamma) = \text{clip}(\mathbf{W}, \sigma(\beta)\min(\mathbf{W}), \sigma(\gamma)\max(\mathbf{W})) \quad (2)$$

where β and γ are learnable parameters for clipping and σ is the sigmoid function.

3 Observation: Rotation Sharpens Weight Distribution



(a) Per-group kurtosis measured on the 15th key projection weight in LLaMA-2 7B model before and after random Hadamard transform with layernorm fusion.



(b) Per-group kurtosis measured on the input activation of the 15th key projection weight in the same manner as 3a in LLaMA-2 7B model. Due to a large difference of average value, the y axis is presented in log scale. Since almost all groups had small negative kurtosis value after transform, we take the absolute value of them.

Figure 3: Kurtosis analysis results to demonstrate the effect of random rotation on model weight and activation.

As shown in Fig. 1, simply applying rotation techniques before LLM quantization can’t guarantee the performance in extremely low-bit scenarios like W2A4. Building on SmoothQuant (Xiao et al., 2023)’s insights, outlier suppression methods improve quantization possibility in the activation space while accepting modest weight space compromises. But recent rotation based PTQ techniques predominantly emphasize the advantages in the activation space, not the disadvantages in the weight space. While rotation-based PTQ techniques work well for moderate quantization up to W4, at W2, the quantization possibility significantly drops.

In this section, we analyze quantization possibility after random Hadamard transformation in both weight and activation spaces in LLaMA-2 7B model. Kurtosis, which measures the fourth standardized moment of a distribution, serves as a key indicator for evaluating outlier frequency and concentration (Lee et al., 2024) that intensify the difficulties in quantization. We selected the 15th key projection module for analysis because it showed one of the highest mean squared errors (MSE) when comparing the distributions before and after transformation among all modules. We analyze kurtosis of weight and input activation in group size of 128 following their channels to fully consider the effects of groupwise quantization configuration used in most quantization methods.

Our analysis in Fig. 3b reveals that rotation effectively distributes activation values along their channel direction, similar to methods like SliceGPT (Ashkboos et al., 2024a), QuaRot (Ashkboos et al., 2024b) and PrefixQuant (Chen et al., 2024a). The original space shows infinite kurtosis due to extreme outliers, while the rotated space shows predominantly near-zero values. From the perspective of per-channel uniform quantization in the activation, the transformation reduces quantization error compared to the original space.

Conversely, our analysis in Fig. 3a shows contrasting circumstances. After going through essential processes such as LayerNorm Fusion and Random Hadamard Transformation, an initially platykurtic distribution with mean kurtosis near 1 becomes more leptokurtic with mean kurtosis near 3.75. These observations indicate that the weight distribution deviates further from the uniform distribution, leading to significant quantization errors when using W2 uniform quantizers, as most weights cluster in two center quantization bins. This finding motivates the development of non-uniform quantizers to optimize bin width distributions. This analysis also explains why FP3 variants outperform INT3 quantization in W3 regime, as NF3’s approach better handles bell-shaped weight distributions, as demonstrated in AFPQ (Zhang et al., 2023).

4 Methodology

We propose a non-linear weight quantization (Section 4.1), an efficient dequantization for non-linear weight partitions (Section 4.2), and a GPU inference kernel for extreme low-bit weights (Section 4.4).

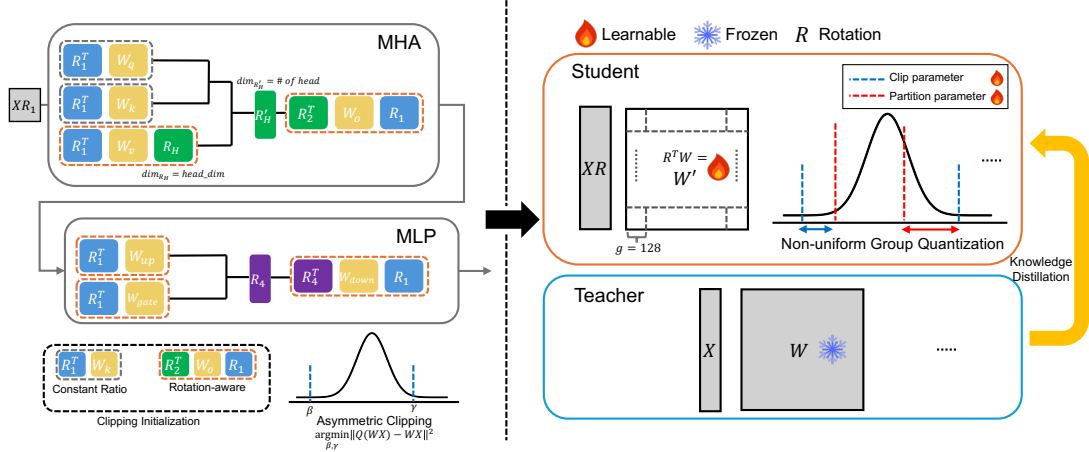


Figure 4: An overview of our QAT-based KD framework of RCP. RCP performs rotation-aware clipping, followed by learnable non-uniform quantization (LDP). During this process, knowledge distillation is employed as the training method.

4.1 Differentiable Non-uniform INT2 Group Quantizer

Rotation-aware Clipping Initialization We initialize clipping parameters in a rotation-aware manner as follows:

$$\operatorname{argmin}_{\beta, \gamma} \|Q(W_R)\mathbf{X}_R - \mathbf{W}_R\mathbf{X}_R\|^2 \quad (3)$$

where $\mathbf{W}_R = R_{front}^T f(\mathbf{W}, \beta, \gamma) R_{rear}$ is the weight matrix obtained by applying appropriate rotations after the clipping f in Eqn. 2. For instance, R_{front} and R_{rear} are set to R_1 and I for up and gate projections, respectively. Rotation configuration for the other types of weights can be found on the left side of Fig. 4.

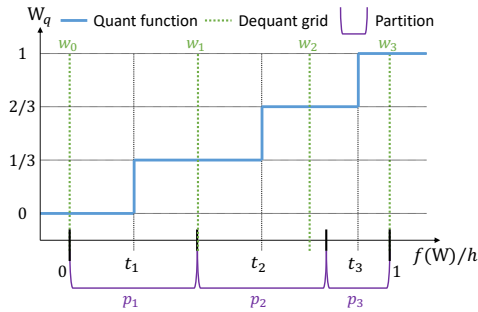


Figure 5: A diagram of Learnable Direct Partitioning (LDP).

Learnable Direct Partitioning The key component of our proposed RCP is a weight quantizer module named learnable direct partitioning (LDP). In order to realize asymmetric weight quantization, we determine value range by LWC and the partitions within the value range by LDP. LDP starts by normalizing the weight \mathbf{W} by a dynamic range $h = \sigma(\gamma)\max(\mathbf{W}) - \sigma(\beta)\min(\mathbf{W})$ determined by the LWC. In LDP, two partitioning variables s_1 and

s_2 are introduced per weight group², which split the range h into three subsections.

$$\begin{aligned} p_1 &= \sigma(s_1), p_2 = (1 - p_1)\sigma(s_2), \\ p_3 &= (1 - p_1)(1 - p_2) \end{aligned} \quad (4)$$

As shown in Fig. 5 and Eqn. 4, s_1 defines the portion of the first partition p_1 in the whole dynamic range h . s_2 defines the portion of the second partition p_2 from the remaining range $(1 - p_1)h$. The third one is trivially calculated. This formulation guarantees that i) the dynamic range h is seamlessly filled out, ii) each portion is constrained between 0 and 100% via the sigmoid reparametrization, and iii) no matter how the parameters are updated, the order of the partitions stays the same. The partitioning parameters are initialized as $s_1 = \sigma^{-1}(1/3)$ and $s_2 = \sigma^{-1}(1/2) = 0$ to evenly split the quantization range in the beginning. The AWQ-styled grid search (Lin et al., 2024a) can also be used to find the optimal partition widths; however, the computational burden will grow exponentially since we have to iterate over a four-dimensional loop (two for LWC and two for LDP).

The quantization process of our LDP can then be derived as follows:

$$\mathbf{W}_q = u\left(\frac{\mathbf{W}}{h} - t_1\right) + u\left(\frac{\mathbf{W}}{h} - t_2\right) + u\left(\frac{\mathbf{W}}{h} - t_3\right) \quad (5)$$

where $u(x)$ is the step function and transition point t_i (i.e., the right edge of each quantization bin) is set to the center of each partition, computed as $t_1 = p_1/2$ and $t_i = t_{i-1} + (p_{i-1} + p_i)/2$.

²For brevity, we do not use a separate notation for group quantization unless necessary since our method can be applied likewise simply by reshaping a weight so that the last dimension becomes the group size.

The straight-through estimator is applied to all step functions so that every parameter (including LLM weights, clipping, and partitioning parameters) can be updated via backpropagation.

4.2 Dequantization for Non-Linear Weight Partitions

Unlike the usual uniform quantization scheme, mapping the quantized weights back to real values is not trivial in NU quantizers as the design space of NU dequantization method is large and the inference pipeline is directly affected. In NU2U (Liu et al., 2022), the quantized weight \mathbf{W}_q is simply dequantized to a uniform grid. Similarly, LLT (Wang et al., 2022) trains a learnable lookup table for weight and activation to adjust the quantization bin widths but keeps the dequantization the same as other common uniform quantizers.

This design choice has an obvious advantage: Inference can be done on existing hardware without any modification. However, we propose non-uniform dequantization as described in Eqn. 6, based on our observation that uniform dequantization can lead to performance drop under extremely low bit configurations, especially on smaller models.

$$\begin{aligned} \mathbf{W}_{deq} = & \sigma(\beta)\min(\mathbf{W}) \\ & + \frac{h}{3} \left(u\left(\frac{\mathbf{W}}{h} - t_1\right)(w_1 - w_0) \right. \\ & + u\left(\frac{\mathbf{W}}{h} - t_2\right)(w_2 - w_1) \\ & \left. + u\left(\frac{\mathbf{W}}{h} - t_3\right)(w_3 - w_2) \right) \end{aligned} \quad (6)$$

The procedure is designed upon Eqn. 5 with several modifications. The value range is shifted and scaled from $[0, 1]$ to $[\sigma(\beta)\min(\mathbf{W}), \sigma(\gamma)\max(\mathbf{W})]$. The dequantization grid w_i is defined in Eqn. 7; the first and last values are the minimum and maximum values of the normalized weight and the middle values are set to the center of the two consecutive transition points.

$$w_i = \begin{cases} 0, & \text{if } i = 0 \\ \frac{t_i + t_{i+1}}{2}, & \text{if } 0 < i < 3 \\ 1, & \text{if } i = 3 \end{cases} \quad (7)$$

The dequantization LUT for a quantization unit (a weight group of size 128 in this paper’s experiments) can be pre-computed without any runtime overhead as follows:

$$\hat{\mathbf{W}} = \{\hat{\mathbf{W}}_0, \hat{\mathbf{W}}_1, \hat{\mathbf{W}}_2, \hat{\mathbf{W}}_3\} \quad (8)$$

where $\hat{\mathbf{W}}_i = \sigma(\beta)\min(\mathbf{W}) + h \cdot w_j$.

4.3 An NF3 Variant of LDP

We apply not only 2-bit weight quantization but also 3-bit quantization using the asymmetric NF format of AFPQ (Zhang et al., 2023) where separate scale values are computed for the negative and positive weights ($s_{neg} = \max(|\mathbf{W}_{neg}|)$, $s_{pos} = \max(\mathbf{W}_{pos})$). Although shown effective, such NF3 quantizer can lead to suboptimal performance when the distribution is not zero-centered. Therefore, we make a further improvement by applying the proposed LDP to this situation.

The idea is to employ the same learnable clipping parameters (β , γ) to obtain the quantization range h and one partitioning parameter s_1 to express the learnable center point as $c = \sigma(\beta)\min(\mathbf{W}) + h \cdot \sigma(s_1)$. Then, the two scale values are updated as follows:

$$\begin{aligned} s_{neg} &= |c - \sigma(\beta)\min(\mathbf{W})|, \\ s_{pos} &= |\sigma(\gamma)\max(\mathbf{W}) - c|, \end{aligned} \quad (9)$$

and the quantization process is derived as follows:

$$\mathbf{W}_q = \begin{cases} \lfloor \frac{\mathbf{W}-c}{s_{pos}} \rfloor, & \text{if } \mathbf{W} > c \\ \lfloor \frac{\mathbf{W}-c}{s_{neg}} \rfloor, & \text{otherwise.} \end{cases} \quad (10)$$

The dequantization is done simply by multiplying the scales to \mathbf{W}_q and adding c .

4.4 W2A4 Look-up Table (LUT) Inference

Designing the inference pipeline of non-uniform W2A4-quantized models poses a big challenge. First, efficient INT tensor cores cannot be utilized since accumulating the multiplication results in INT quantized space makes it impossible to dequantize the weights back to correct non-uniform real values in the LUT $\hat{\mathbf{W}}$. Second, both weights and activations must undergo online dequantization to support dynamic quantization, which adds a large amount of computation overhead.

Therefore, we focus on designing GEMV kernel for LUT decoding predominantly bounded by memory bandwidth, which is ideal for featuring the advantage of extreme W2A4KV4 compression. We report our early exploration on GEMM design in Section A.5.

Kernel Arguments and Block Tiling We define the input channel dimension as C , the output channel dimension as H , and the number of groups per channel as N . The quantized activation tensor \mathbf{X}_q has a shape of $1 \times C/2$ and is INT8, with each element holding two INT4 activation elements. The

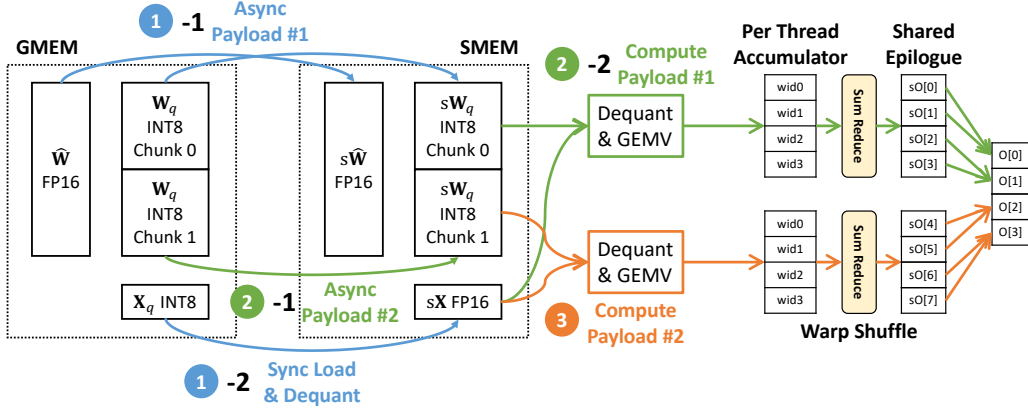


Figure 6: An overview of our GPU GEMV kernel with data path along memory hierarchy, pipelining, and epilogue concisely illustrated. wid is the warp index and the per-thread accumulator is simplified (warp lane dimension is not shown).

activation scale S is an FP16 scalar. The quantized weight tensor W_q has a shape of $H \times C/4$ and is INT8, with each element holding four UINT2 weights. The dequantization grid \hat{W} has a shape of $H \times N/4$ and is FP16. The output activation O is an FP16 tensor of shape $1 \times H$.

Each thread block consists of 128 threads (4 warps) and we only tile along the output dimension and define the tile size as BH . The reason we do not follow the traditional 2-dimensional tiling is that both the input tokens and weights are stored in row-major format and have sub-byte packing along the column direction, which makes it hard to efficiently use high-bandwidth memory that performs best when reading 128B data consecutively. Also, global loads with small transactions and repeated shared stores complicate the pipeline design for latency hiding and degrade overall performance.

Data Path and Latency Hiding Pipeline As demonstrated in Fig. 6, we store the dequantized input activation sX ($1 \times C$, FP16), the quantized weight tile sW_q ($BH \times C/4$, INT8), the corresponding dequantization grid tile $s\hat{W}$ ($BH \times N/4$, FP16), and a shared output array sO (1×8 , FP16) in shared memory.

To make our kernel efficient via latency hiding, we design a pipelining strategy where a thread block handles a half of the output elements ($BH/2$) and iterates twice. At the beginning, an asynchronous copy of \hat{W} and the first W_q chunk (of size $BH/2 \times C/4$) is issued using `cp.async` instruction (1-1 in Fig. 6). Simultaneously, X_q is synchronously loaded from global memory and dequantized to be stored into sX (1-2), overlapping activation dequantization latency with loading the

first weight chunk.

Subsequently, while we bring in the second W_q chunk using `cp.async` (2-1), we perform dequantization, inner product, and warp reduce on the first W_q chunk at the same time (2-2), thereby hiding the second chunk loading latency with computation of the first chunk. Finally, the computation on the second chunk is performed (3) and the shared output array is reduced once more if necessary.

Additional details (e.g., dequantization implementation, shared output) not mentioned here are provided in Section A.6.

5 Experiments

5.1 Experimental Settings

Models and Tasks We evaluate RCP on LLaMA-1 (Touvron et al., 2023a) 7B, LLaMA-2 (Touvron et al., 2023b) 7B, LLaMA-3 (AI@Meta, 2024)(1B, 3B, 8B). Our evaluation of RCP was carried out on PIQA (Bisk et al., 2020), HelLaSwag (Zellers et al., 2019), WinoGrande (Sakaguchi et al., 2021), ARC-c (Clark et al., 2018) and MMLU (Hendrycks et al., 2020). We use LLM-Humaneval-Benchmarks (Chen et al., 2021) and GSM8K (Cobbe et al., 2021) for reasoning tasks evaluation. We also report the perplexity score on WikiText2 (Merity et al., 2016) for our evaluation.

Training Data For a fair comparison with our baseline, we use the instruction-tuning data from Alpaca (Taori et al., 2023) and the training set of WikiText2 for general language tasks. For understanding and generating code, we use Evol-Instruct-Code³. For math reasoning we use Meta-

³<https://github.com/nickrosh/evol-teacher>

#Bits (W-A-KV)	Configuration			LLaMA-1 7B			LLaMA-2 7B			LLaMA-3 8B			LLaMA-3.2 1B			LLaMA-3.2 3B		
	Method	Rotation	LDP	MMLU	0-shot [†]	Wiki [†]	MMLU	0-shot [†]	Wiki [†]	MMLU	0-shot [†]	Wiki [†]	MMLU	0-shot [†]	Wiki [†]	MMLU	0-shot [†]	Wiki [†]
16-16-16				35.10	68.40	5.68	46.45	61.67	5.47	68.40	72.93	6.10	32.20	58.90	9.74	58.00	65.30	7.82
2-4-16	BitDistiller			25.88	42.56	23.19	26.24	43.36	16.47	23.11	39.46	Inf	25.00	36.82	Inf	24.41	37.89	Inf
	Ours	✓		26.75	52.28	8.79	26.04	51.49	8.93	29.80	50.59	13.68	25.00	41.08	31.32	29.60	45.29	18.79
	Ours	✓	✓	26.98	52.46	8.28	28.04	51.10	8.18	31.87	50.86	12.48	26.30	41.35	27.46	31.40	45.71	16.96
2-4-4	BitDistiller			24.45	43.08	19.98	26.59	44.93	17.40	23.29	39.75	Inf	24.66	37.55	Inf	24.62	37.26	Inf
	Ours	✓		26.98	52.21	8.92	26.41	51.10	8.93	29.66	49.80	14.05	24.74	40.77	33.86	31.44	44.26	19.58
	Ours	✓	✓	27.34	52.29	8.28	26.92	51.22	8.31	31.01	50.41	12.69	25.62	41.80	29.30	30.33	45.56	17.52
3-4-16	BitDistiller			26.88	55.68	7.47	31.72	56.15	7.04	42.24	55.39	10.19	26.06	37.53	Inf	25.22	37.32	Inf
	Ours	✓		28.70	58.52	6.44	34.30	59.28	6.25	54.16	61.06	7.92	26.45	47.88	13.75	47.34	55.66	9.82
	Ours	✓	✓	29.46	59.39	6.39	37.33	59.74	6.23	55.33	61.53	7.80	27.77	48.18	13.68	47.31	55.87	9.74
3-4-4	BitDistiller			27.04	56.05	7.54	30.19	55.51	7.15	40.70	56.35	10.46	25.48	38.75	Inf	25.91	37.27	Inf
	Ours	✓		28.80	58.48	6.45	33.46	58.53	6.36	51.74	59.69	8.04	26.11	47.14	14.58	46.08	55.08	10.05
	Ours	✓	✓	30.00	58.55	6.39	36.07	59.27	6.33	52.55	61.11	7.95	26.54	47.71	14.44	46.40	55.12	9.99

Table 1: Comparison of the perplexity score on WikiText2, MMLU (5s), and 0-shot[†]. 0-shot[†] is average score of 4 Zero-shot Common Sense Reasoning tasks. We show the perplexity results >100 by Inf. Full results of Zero-shot tasks are in the Appendix.

MathQA (Yu et al., 2023).

Experiment Configuration We compare our proposed RCP with the state-of-the-art QAT method, BitDistiller (Du et al., 2024). We employ a symmetric uniform quantizer for activations and an asymmetric uniform quantizer with a group size of 128 for KV-cache. Clipping ratio is set to 0.9 and 0.95 for activations and KV-cache, respectively. We set the weight learning rate to 8e-7 for W/A4 and 1e-6 for W/A4KV4, while the learning rate for LWC and LDP was set to 1e-5. All training was conducted for 8 epochs, using a batch size of 4 or 8. We set the training sequence length to 1k and the evaluation sequence length to 2k.

5.2 Results

Language Modeling Tasks The results are summarized in Table 1. From the perspective of general language tasks, our method demonstrates the ability to quantize activations and KV-cache under the W2 settings to 4-bit, which was previously unattainable using existing QAT methods. The application of rotation effectively addresses the outlier issues, a common bottleneck in quantization, enabling stable performance even in extremely low-bit quantization scenarios. Furthermore, the addition of LDP not only improves performance on general language tasks but also enhances the accuracy of zero/few shot tasks, which were not adequately addressed by rotation alone. In case of LLaMA-2 7B W2A4KV4, a performance degradation is observed when using rotation only compared to the baseline. However, by incorporating LDP, consistent performance improvements were achieved.

Reasoning Tasks The results of the reasoning tasks are summarized in Table 2. We evaluate rea-

#Bits (W-A-KV)	Configuration			WizardCoder 7B		MetaMath 7B	
	Method	Rotation	LDP	HumanEval	GSM8K		
16-16-16				54.88	66.41		
2-4-16	BitDistiller			2.43	0.0		
	Ours	✓		14.63	1.25		
	Ours	✓	✓	27.44	41.64		
2-4-4	BitDistiller			3.50	5.39		
	Ours	✓		6.09	0.16		
	Ours	✓	✓	23.20	40.16		
3-4-16	BitDistiller			0.0	0.0		
	Ours	✓		39.02	0.0		
	Ours	✓	✓	40.85	54.69		
3-4-4	BitDistiller			0.0	0.0		
	Ours	✓		41.46	0.0		
	Ours	✓	✓	43.29	52.73		

Table 2: Reasoning task results of RCP on domain-specific LLMs.

soning capabilities in the domains of coding and mathematics.

For the coding domain-specific model, WizardCoder (Luo et al., 2023), BitDistiller failed to offer the functional quantized models in both W3 and W2 settings. In our method, applying rotation alone was not effective in W2 settings and recovered some output quality in W3 settings. By incorporating LDP, we achieved up to a threefold improvement in performance, with accuracy increasing from 6.09% to 23.20% under the W2A4KV4 configuration. As shown in Fig. 8 with the application of LDP, we were able to produce logically correct code outputs and eliminate repetition of meaningless code generation.

For the mathematical reasoning model, MetaMath (Yu et al., 2023), the baseline BitDistiller and ours without LDP failed to offer functional quantized models while ours with LDP could produce working quantized models. These results highlight the critical role of LDP in enabling proper task performance for reasoning models under extreme low-bit quantization. The output comparison for this task is summarized in Fig. 2.

Layer Size	(2048, 2048)	(3072, 3072)	(4096, 4096)
FP16	0.042	0.047	0.051
QuaRot	0.077	0.057	0.078
QuaRot+FP16Had	0.158	0.210	0.159
QuaRot+FP32Had	0.194	0.238	0.191
RCP	0.028	0.03	0.040
RCP+FP16Had	0.114	0.167	0.110
RCP+FP32Had	0.136	0.204	0.148

Table 3: GEMV latency without activation quantization overhead. The layer size is composed as (input channel, output channel). All latency numbers are in milliseconds. Full results are in the Appendix.

	3.2-1B	3.2-3B	1.2-7B	3-8B
FP16	2.47GB	6.43GB	13.48GB	16.06GB
RCP W3	1.46GB (1.69x)	2.77GB (2.32x)	3.26GB (4.14x)	5.05GB (3.18x)
RCP W2	1.35GB (1.82x)	2.46GB (2.62x)	2.55GB (5.29x)	4.28GB (3.75x)

Table 4: Memory footprint comparison for different weight precisions. Note that 1.2-7B refers to LLaMA-1 and LLaMA-2.

Inference Table 3 and 4 present the results for GEMV in terms of latency and memory consumption. The latency of GEMV, excluding the activation quantization overhead, is faster compared to FP16 and QuaRot (Ashkboos et al., 2024b). This improvement can be attributed to the lower bit precision, which enhances computational efficiency. Table 4 measures the peak memory footprint for W2A4 and W3A4. For W2A4, a significant reduction on 5.29x in memory footprint was achieved compared to FP16. Note that in the LLaMA-3.2 series, it is necessary to separate the embedding table and head modules to satisfy the invariance arising from their tying. Furthermore, as the size of the embedding table has increased compared to previous models, the compression ratio has decreased accordingly.

5.3 Ablation Studies

#Bits	Rotation	LWC	LDP	PPL \downarrow
2-4-4				17.40
	✓			8.93
	✓	✓		10.59
	✓	✓	✓	8.31

Table 5: Ablation study on the impact of each component of our proposed RCP on performance for LLaMA-2 7B.

Impact of RCP Components As shown in Table 5, we conducted an ablation study to analyze the impact of removing each component of RCP on model performance. In 4-bit activation quantization, addressing the outliers in activations was crucial, and this was effectively resolved using rotation, which led to the largest performance gain

compared to the baseline. This demonstrates that rotation is a viable solution when quantizing activations to low bit-width.

However, we found that the narrow weight distribution caused by rotation hindered successful training of LWC. Specifically, when examining the training process with rotation applied during LWC training, the training loss curve exhibited instability. The combination of low bit-width quantization challenges and the difficulty in finding an optimal LWC required training stabilization, which was achieved by LDP. LDP reduced PPL from 10.59 to 8.31, demonstrating a clear advantage.

W2A4KV4	PPL \downarrow
RCP	8.31
- R_3	8.48
- $[R_2, R_3]$	8.83
- $[R_3, R_4]$	12.24
- $[R_2, R_3, R_4]$	12.76
- $[R_1, R_2, R_3, R_4]$	25.05

Table 6: Ablation study on the impact of rotation configuration for LLaMA-2 7B.

Impact of Rotation Configuration Since the rotation requires additional processes before and after inference, we investigated the performance trend by incrementally adding rotation matrices (R_1, R_2, R_3, R_4) to different components to find an appropriate balance between accuracy and overhead. The results are presented in Table 6. The table demonstrates that the impact of the rotation was most significant with R_1 and R_4 . Especially, R_1 , which applies rotation matrix to the input weight and input activation of all modules thereby having the largest impact on quantization performance. Additionally, our analysis revealed that in LLaMA-2 7B, the input to the down projection layer (of the MLP) exhibited a significant number of outliers, which was effectively addressed through R_4 online rotation to activation.

6 Conclusion

RCP enables weights to be quantized to extreme low-bit precision through learnable non-uniform quantization while harmonizing with rotation to optimize both activations and KV-cache to 4-bit. RCP has achieved the first W2A4KV4 configuration and implemented optimized kernels for inference, facilitating LLM serving even in resource-constrained environments.

Limitations

Although our proposed RCP first enables challenging W2A4KV4 quantization of commonly used LLM models, we report key limitations of our work.

First, the online rotation operators (R_2 through R_4) inevitably introduce additional latency for training and evaluation. Custom CUDA kernels or FlashAttention3 (Shah et al., 2024) can minimize such speed-down, however, it might not be a viable option for many edge application scenarios where no hardware support for fast Hadamard transform is available.

Second, RCP requires heavier hyperparameter tuning than BitDistiller since rotation tends to make the model weights more sensitive to the choice of learning rate. This can be prohibitive when a user is under a strict budget limit.

In future work, we could explore applying an optimized rotation matrix that achieves comparable performance to Cayley-optimized rotation matrices used in SpinQuant (Liu et al., 2024b) while maintaining similar computational costs to the Random Hadamard rotation matrices employed in QuaRot (Ashkboos et al., 2024b).

References

AI@Meta. 2024. [Llama 3 model card](#).

Saleh Ashkboos, Maximilian L. Croci, Marcelo Gennari do Nascimento, Torsten Hoefler, and James Hensman. 2024a. [SliceGPT: Compress large language models by deleting rows and columns](#). In *The Twelfth International Conference on Learning Representations*.

Saleh Ashkboos, Amirkeivan Mohtashami, Maximilian L Croci, Bo Li, Martin Jaggi, Dan Alistarh, Torsten Hoefler, and James Hensman. 2024b. [Quarot: Outlier-free 4-bit inference in rotated llms](#). *arXiv preprint arXiv:2404.00456*.

Yonatan Bisk, Rowan Zellers, Jianfeng Gao, Yejin Choi, et al. 2020. [Piqa: Reasoning about physical commonsense in natural language](#). In *Proceedings of the AAAI conference on artificial intelligence*, volume 34, pages 7432–7439.

Mark Chen, Jerry Tworek, Heewoo Jun, Qiming Yuan, Henrique Ponde De Oliveira Pinto, Jared Kaplan, Harri Edwards, Yuri Burda, Nicholas Joseph, Greg Brockman, et al. 2021. [Evaluating large language models trained on code](#). *arXiv preprint arXiv:2107.03374*.

Mengzhao Chen, Yi Liu, Jiahao Wang, Yi Bin, Wenqi Shao, and Ping Luo. 2024a. [Prefixquant: Static quantization beats dynamic through prefixed outliers in llms](#). *arXiv preprint arXiv:2410.05265*.

Mengzhao Chen, Wenqi Shao, Peng Xu, Jiahao Wang, Peng Gao, Kaipeng Zhang, Yu Qiao, and Ping Luo. 2024b. [Efficientqat: Efficient quantization-aware training for large language models](#). *arXiv preprint arXiv:2407.11062*.

Jungwook Choi, Zhuo Wang, Swagath Venkataramani, Pierce I-Jen Chuang, Vijayalakshmi Srinivasan, and Kailash Gopalakrishnan. 2018. [Pact: Parameterized clipping activation for quantized neural networks](#). *Preprint*, arXiv:1805.06085.

Peter Clark, Isaac Cowhey, Oren Etzioni, Tushar Khot, Ashish Sabharwal, Carissa Schoenick, and Oyvind Tafjord. 2018. [Think you have solved question answering? try arc, the ai2 reasoning challenge](#). *arXiv preprint arXiv:1803.05457*.

Karl Cobbe, Vineet Kosaraju, Mohammad Bavarian, Mark Chen, Heewoo Jun, Lukasz Kaiser, Matthias Plappert, Jerry Tworek, Jacob Hilton, Reiichiro Nakano, Christopher Hesse, and John Schulman. 2021. [Training verifiers to solve math word problems](#). *arXiv preprint arXiv:2110.14168*.

Dayou Du, Yijia Zhang, Shijie Cao, Jiaqi Guo, Ting Cao, Xiaowen Chu, and Ningyi Xu. 2024. [Bitdistiller: Unleashing the potential of sub-4-bit llms via self-distillation](#). *arXiv preprint arXiv:2402.10631*.

Elias Frantar, Saleh Ashkboos, Torsten Hoefler, and Dan Alistarh. 2022. [Optq: Accurate quantization for generative pre-trained transformers](#). In *The Eleventh International Conference on Learning Representations*.

Han Guo, William Brandon, Radostin Cholakov, Jonathan Ragan-Kelley, Eric P. Xing, and Yoon Kim. 2024. [Fast matrix multiplications for lookup table-quantized llms](#). *Preprint*, arXiv:2407.10960.

Dan Hendrycks, Collin Burns, Steven Basart, Andy Zou, Mantas Mazeika, Dawn Song, and Jacob Steinhardt. 2020. [Measuring massive multitask language understanding](#). *arXiv preprint arXiv:2009.03300*.

Sehoon Kim, Coleman Richard Charles Hooper, Amir Gholami, Zhen Dong, Xiuyu Li, Sheng Shen, Michael W. Mahoney, and Kurt Keutzer. 2024. [SqueezeLLM: Dense-and-sparse quantization](#). In *Forty-first International Conference on Machine Learning*.

Janghwan Lee, Jiwoong Park, Jinseok Kim, Yongjik Kim, Jungju Oh, Jinwook Oh, and Jungwook Choi. 2024. [Amx4: Taming activation outliers with asymmetric microscaling floating-point for 4-bit llm inference](#). *Preprint*, arXiv:2411.09909.

- Ji Lin, Jiaming Tang, Haotian Tang, Shang Yang, Wei-Ming Chen, Wei-Chen Wang, Guangxuan Xiao, Xingyu Dang, Chuang Gan, and Song Han. 2024a. Awq: Activation-aware weight quantization for llm compression and acceleration. In *MLSys*.
- Yujun Lin, Haotian Tang, Shang Yang, Zhekai Zhang, Guangxuan Xiao, Chuang Gan, and Song Han. 2024b. [Qserve: W4a8kv4 quantization and system co-design for efficient llm serving](#). *Preprint*, arXiv:2405.04532.
- Zechun Liu, Kwang-Ting Cheng, Dong Huang, Eric P Xing, and Zhiqiang Shen. 2022. Nonuniform-to-uniform quantization: Towards accurate quantization via generalized straight-through estimation. In *Proceedings of the IEEE/CVF conference on computer vision and pattern recognition*, pages 4942–4952.
- Zechun Liu, Barlas Oguz, Changsheng Zhao, Ernie Chang, Pierre Stock, Yashar Mehdad, Yangyang Shi, Raghuraman Krishnamoorthi, and Vikas Chandra. 2024a. Llm-qat: Data-free quantization aware training for large language models. *arXiv preprint arXiv:2305.17888*.
- Zechun Liu, Changsheng Zhao, Igor Fedorov, Bilge Soran, Dhruv Choudhary, Raghuraman Krishnamoorthi, Vikas Chandra, Yuandong Tian, and Tijmen Blankevoort. 2024b. Spinquant–llm quantization with learned rotations. *arXiv preprint arXiv:2405.16406*.
- Ziyang Luo, Can Xu, Pu Zhao, Qingfeng Sun, Xubo Geng, Wenxiang Hu, Chongyang Tao, Jing Ma, Qingwei Lin, and Daxin Jiang. 2023. Wizardcoder: Empowering code large language models with evol-instruct. *arXiv preprint arXiv:2306.08568*.
- Stephen Merity, Caiming Xiong, James Bradbury, and Richard Socher. 2016. Pointer sentinel mixture models. *arXiv preprint arXiv:1609.07843*.
- Keisuke Sakaguchi, Ronan Le Bras, Chandra Bhagavatula, and Yejin Choi. 2021. Winogrande: An adversarial winograd schema challenge at scale. *Communications of the ACM*, 64(9):99–106.
- Jay Shah, Ganesh Bikshandi, Ying Zhang, Vijay Thakkar, Pradeep Ramani, and Tri Dao. 2024. Flashattention-3: Fast and accurate attention with asynchrony and low-precision. *arXiv preprint arXiv:2407.08608*.
- Wenqi Shao, Mengzhao Chen, Zhaoyang Zhang, Peng Xu, Lirui Zhao, Zhiqian Li, Kaipeng Zhang, Peng Gao, Yu Qiao, and Ping Luo. 2024. [Omniquant: Omnidirectionally calibrated quantization for large language models](#). In *The Twelfth International Conference on Learning Representations*.
- Rohan Taori, Ishaan Gulrajani, Tianyi Zhang, Yann Dubois, Xuechen Li, Carlos Guestrin, Percy Liang, and Tatsunori B. Hashimoto. 2023. Stanford alpaca: An instruction-following llama model. https://github.com/tatsu-lab/stanford_alpaca.
- Hugo Touvron, Thibaut Lavril, Gautier Izacard, Xavier Martinet, Marie-Anne Lachaux, Timothée Lacroix, Baptiste Rozière, Naman Goyal, Eric Hambro, Faisal Azhar, et al. 2023a. Llama: Open and efficient foundation language models. *arXiv preprint arXiv:2302.13971*.
- Hugo Touvron, Louis Martin, Kevin Stone, Peter Albert, Amjad Almahairi, Yasmine Babaei, Nikolay Bashlykov, Soumya Batra, Prajjwal Bhargava, Shruti Bhosale, et al. 2023b. Llama 2: Open foundation and fine-tuned chat models. *arXiv preprint arXiv:2307.09288*.
- Longguang Wang, Xiaoyu Dong, Yingqian Wang, Li Liu, Wei An, and Yulan Guo. 2022. Learnable lookup table for neural network quantization. In *Proceedings of the IEEE/CVF conference on computer vision and pattern recognition*, pages 12423–12433.
- Guangxuan Xiao, Ji Lin, Mickael Seznec, Hao Wu, Julien Demouth, and Song Han. 2023. Smoothquant: Accurate and efficient post-training quantization for large language models. In *Proceedings of the 40th International Conference on Machine Learning*.
- Longhui Yu, Weisen Jiang, Han Shi, Jincheng Yu, Zhengying Liu, Yu Zhang, James T Kwok, Zhengguo Li, Adrian Weller, and Weiyang Liu. 2023. Metamath: Bootstrap your own mathematical questions for large language models. *arXiv preprint arXiv:2309.12284*.
- Rowan Zellers, Ari Holtzman, Yonatan Bisk, Ali Farhadi, and Yejin Choi. 2019. Hellaswag: Can a machine really finish your sentence? *arXiv preprint arXiv:1905.07830*.
- Yijia Zhang, Sicheng Zhang, Shijie Cao, Dayou Du, Jianyu Wei, Ting Cao, and Ningyi Xu. 2023. Afpq: Asymmetric floating point quantization for llms. *arXiv preprint arXiv:2311.01792*.
- Yilong Zhao, Chien-Yu Lin, Kan Zhu, Zihao Ye, Lequn Chen, Size Zheng, Luis Ceze, Arvind Krishnamurthy, Tianqi Chen, and Baris Kasikci. 2024. [Atom: Low-bit quantization for efficient and accurate llm serving](#). *Preprint*, arXiv:2310.19102.

A Appendix

A.1 Related Works

PTQ and QAT GPTQ (Frantar et al., 2022) introduced an accurate post-training quantization (PTQ) method based on approximate second-order information that enables weight-only quantization down to 3-4 bits through block-wise reconstruction. SmoothQuant (Xiao et al., 2023) proposed smoothing activation outliers by offline migrating quantization difficulty from activations to weights through equivalent transformation, enabling accurate 8-bit weight-activation quantization. AWQ (Lin et al.,

2024a) built upon SmoothQuant’s equivalent transformation concept but introduced activation-aware channel-wise scaling to protect salient weights during weight-only quantization. OmniQuant (Shao et al., 2024) enhanced quantization by introducing learnable weight clipping and equivalent transformation parameters that are jointly optimized through block-wise reconstruction.

LLM-QAT (Liu et al., 2024a) was the first to explore quantization-aware training (QAT) for LLMs using data-free knowledge distillation from the full-precision model to guide low-bit quantization. Bit-Distiller (Du et al., 2024) improved upon LLM-QAT by introducing a self-distillation framework with confidence-aware KL divergence to enable sub-4-bit quantization while maintaining efficiency. EfficientQAT (Chen et al., 2024b) made QAT more practical by introducing block-wise training of all parameters followed by end-to-end training of quantization parameters.

Rotation QuaRot (Ashkboos et al., 2024b) introduced a rotation-based approach using Hadamard transformations to eliminate outliers in activations and KV-cache, enabling end-to-end 4-bit quantization including weights, activations and KV-cache. SpinQuant (Liu et al., 2024b) enhanced this rotation-based approach by learning optimal rotation matrices instead of using random ones.

Non-uniform Quantization PACT (Choi et al., 2018) introduced a learnable clipping parameter for activation quantization during training to help preserve model accuracy. SqueezeLLM (Kim et al., 2024) took a different direction by focusing on identifying and extracting outlier values into a sparse format while quantizing the remaining dense values. NU2U (Liu et al., 2022) proposed learning flexible non-uniform input thresholds while maintaining uniform output levels to balance quantization accuracy with hardware efficiency.

Serving Optimization Atom (Zhao et al., 2024) first introduced W4A4 quantization for LLM serving but faced performance challenges from dequantization overhead. QServe (Lin et al., 2024b) addressed the challenges by introducing W4A8KV4 quantization with progressive group quantization FLUTE (Guo et al., 2024) focused on developing efficient GPU kernels for flexible lookup table-based quantization methods that can support arbitrary bit widths including 3-bit and 4-bit quantization.

A.2 Reasoning Task Example: HumanEval

We evaluate the capability of the WizardCoder 7B model to generate solutions for coding problems. The results are presented in Fig. 8. The orange box in Fig. 8 represent the model output after applying rotation and quantizing the weights to W2A4KV4 using a uniform asymmetric quantizer. Under uniform quantization, it is evident that the model fails to perform logical generation tasks even applying rotation; it merely produces the structural template of code without generating functionality correct code. In contrast, the green box shows the results when the weights are quantized to W2A4KV4 using LDP. Unlike the uniform quantizer, the LDP approach yields code that not only adheres faithfully to the given instructions and generates a functionality correct algorithm, but also provides detailed explanatory comments. While perplexity on standard language modeling tasks did not reveal significant differences between the two cases, these findings suggest that LDP plays a crucial role in enabling logical reasoning tasks under extreme low-bit quantization.

A.3 Implementation Details

All model parameters are in BF16 format throughout training and evaluation since we observe overflow in the hidden activation of the last two FFNs on several models set to FP16.

In existing rotation-based PTQ methods (Ashkboos et al., 2024b; Liu et al., 2024b), rotations are done in FP32 to avoid precision issues. However, this leads to computational overhead due to a large number of typecasting. When fusing rotations to model weights, they are temporarily promoted to FP32, multiplied by an appropriate rotation matrix, and then demoted back to their original precision. For online rotations (R_2 , R_3 , and R_4), all tensors are processed in BF16.

A.4 More Ablation Studies

#Bits	Factorized	Batch	Epoch	PPL [↓]
W2		8	8	7.6
	✓	1	64	12.5

Table 7: Comparison of factorized configurations.

Factorized Rotation In our algorithm, rotation serves as a pre-conditioning tool for reducing outliers in activation and KV-cache. All rotations except the matrices that should be applied online (R_3

and R_4) are fused into the corresponding model weight at the beginning of the QAT process. This means their orthogonality is not guaranteed during backpropagation steps with AdamW optimizer.

We investigate the impact of preserving the orthogonality of the rotations by modifying the LLaMA-2 model implementation to apply all rotation operators online while freezing the rotation matrices. Table 7 presents the results. Applying factorized rotation prevents the fusion of the rotation matrix into the weight tensor, resulting in an increase in the number of intermediate tensors (rotation matrix and intermediate activation), which significantly raises VRAM requirements. For instance, applying only R_1 needs to reduce the training batch size from 8 to 1. Under the condition of maintaining an equal total number of tokens processed by the model, we compared the performance of W2A16KV16 with only R_1 applied. The perplexity of BitDistiller with R_1 fused was 7.6, whereas applying QAT with factorized rotation resulted in a PPL of 12.5. This indicates that performing weight updates through QAT while preserving R_1 orthogonality hinders QAT optimization. This is because the factorization constrains the weight updates to a restricted space defined by the factorized condition, requiring the backpropagation process to maintain within this space. This limitation reduces the flexibility of optimization, making it challenging to efficiently adjust the weights. Consequently, this leads to suboptimal training dynamics and ultimately results in degraded model performance. Furthermore, extending factorization to R_2 and R_4 would lead to an even greater increase in VRAM usage. In contrast, training fused weight effectively alters only the distribution and is analogous to standard LLM training, which is well-known to perform effectively. In summary, given that resource consumption increases while performance degrades, we have decided not to explicitly preserve orthogonality and instead allow the algorithm to handle this aspect.

Layerwise vs. End-to-end QAT Recent work introduced layerwise QAT (Chen et al., 2024b), which updates one layer at a time while freezing others, allowing training on a single GPU. We extended this approach by applying rotation but observed significant performance degradation. The main issue stemmed from fuse rotation matrices in the weights; layerwise updates disrupted orthogonality, preventing the activation space from restor-

ing its original space, leading to cumulative errors and reduced accuracy. In contrast, end-to-end methods like BitDistiller naturally mitigate this issue during updates. While factorized rotation could help, its high GPU memory requirements for holding rotation matrices and intermediate tensors on GPU memory offsets the advantage. Despite these challenges, exploring single GPU training using rotation matrix remains a promising direction for future work.

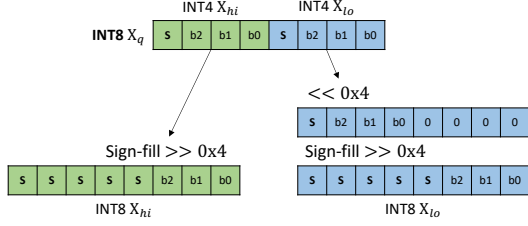
A.5 GEMM Kernel Design for Non-uniform W2A4 Quantization

In our initial GEMM implementation, we attempted to leverage the asynchronous copy to perform dequantization and MMA operations while loading quantized weights and activations, which resulted in slower performance compared to half-precision PyTorch kernel (approx. $480\mu\text{s}$ versus $330\mu\text{s}$ on a single $(4,096 \times 4,096)$ linear layer with 2,048 tokens as input). We suggest two underlying reasons; 1) dequantization requires multiple iterations of shifting, masking, and casting to half-precision instruction, and these are typically expensive on the GPU, further deepening the compute-bound nature of the GEMM problem and 2) packing four quantized weights into a single UINT8 and two quantized activation elements into a single INT8 reduces the width of per-block global memory loads, thereby narrowing the chance for latency hiding. Therefore, we decided to leave the prefill acceleration as future work and instead focus on designing a GEMV kernel to accelerate decoding.

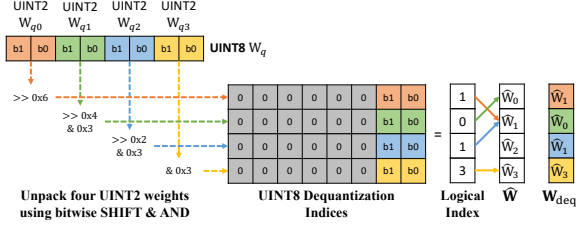
A.6 Details and More Results on GEMV

Online Dequantization and Vectorization Fig. 7 illustrates how the activations and weights are dequantized in our GEMV kernel. For activations, there are two INT4 elements (X_{hi} , X_{low}) in a packed INT8 X_q . For X_{hi} , X_q is copied to an INT8 register, and the register is right-shifted by 4 bits with sign-filling. For X_{low} , X_q is also copied to an INT8 register, which is left-shifted by 4 bits first to put the sign bit of X_{low} to the MSB and then right-shifted by 4 bits with sign filling. This process is shown in Fig. 7a.

For weights, there are four UINT2 elements (W_{q0} , W_{q1} , W_{q2} , W_{q3}) in a packed UINT8 W_q . W_q is copied to 4 UINT8 registers (for each UINT2 element) that are used as indices to look up the LUT \hat{W} . For W_{q0} , the register is right-shifted by 6



(a) Dequantization process of two INT4 activations packed in INT8.



(b) Dequantization process of 4 UINT2 weights packed in UINT8.

Figure 7: Online dequantization of INT4 activations and UINT2 weights.

bits. For W_{q_1} , the register is right-shifted by 4 bits, and a logical AND operation with a bit mask $0x03$ is applied to select only two LSBs. For W_{q_2} , the register is right-shifted by 2 bits and also performs logical AND with a bit mask $0x03$. For W_{q_3} , the register only does a logical AND with a bit mask $0x03$.

The unit dequantization operations can be vectorized to increase memory throughput so that each thread writes 16B of data to shared memory. For activations, 4 X_{q_s} are loaded from global memory at once by type casting via `reinterpret_cast<char4*>`, which produces 8 FP16 dequantized activations to be written in $s\mathbf{X}$. The dequantization is performed the same on each X_q in a `char4` struct. For weights, 2 W_{q_s} are loaded from memory via `reinterpret_cast<uint16_t*>`. Unlike the activation case, the right-shift and logical AND operation can be naturally iterated 8 times to generate 8 FP16 dequantized weights that are directly multiplied to the corresponding activation from $s\mathbf{X}$.

Shared Epilogue As mentioned in Section 4.4, a shared output can be necessary due to our chunking strategy. For example, if BH is 4, then two warps will compute one output element to process a weight chunk of size $BH/2 \times C/4$, and after warp-level sum reduction, the reduced values from the two warps must be summed once again. To imple-

ment this, we allocate a shared output buffer $s\mathbf{O}$ with twice the number of warps.

After the inner product stage for the first weight chunk, each thread in a block will have an FP32 accumulator with a shape of $(4, 32)$. Applying the warp-shuffle primitive `__shfl_xor_sync` 5 times allows us to sum all accumulations to the first thread of each warp without any global nor shared memory access, producing 4 FP32 values to be cast to FP16 and stored in $s\mathbf{O}[0 : 4]$. The first and the last two values are summed up as the first and the second output elements, respectively. Repeating the same process on the second weight chunk will produce the next 4 FP32 values for $s\mathbf{O}[4 : 8]$ to compute the third and the fourth output elements accordingly.

Latency Benchmark Our GEMV kernel is fully written in CUDA 12.1 and compiled for Nvidia A100 SXM 40GB model. We build our benchmarking framework upon QuaRot’s (Ashkboos et al., 2024b) implementation that provides proper PyTorch bindings and a basic activation quantizer that combines a max reduction function written in PyTorch and a symmetric INT quantizer with INT4 sub-byte data handler from CUTLASS⁴.

Since the reduction part is neither a specialized implementation nor compiler-optimized, a huge overhead induced by the QuaRot’s activation quantizer is observed (about $100\mu s$ on average). Therefore in the main results, we assume that the symmetric quantization is natively supported by hardware and replace the quantizer with a dummy class that outputs random quantized activation and scale tensors. The results with the inefficient quantizer implementation are listed in Table 11 and 12 for value and down projection weight, respectively. We also report the latency values without activation overhead for the down projection weight in Table 10.

A.7 Information About Use of AI Assistants

AI assistance was strictly limited to linguistic perspectives, such as grammar and spell checking, and finding synonyms.

⁴<https://github.com/NVIDIA/cutlass>

Model	#Bits (W-A-KV)	Configuration			PIQA	Hella.	Wino.	ARC-c	Avg.	
		Method	Rotation	LDP						
1-7B	16-16-16				79.80	76.10	70.10	47.60	68.4	
	2-4-16	BitDistiller			61.53	35.98	49.25	23.46	43.56	
		Ours	✓		70.67	45.86	62.03	30.54	52.28	
		Ours	✓	✓	70.62	46.41	61.48	31.32	52.46	
	2-4-4	BitDistiller			63.38	34.32	50.82	23.80	43.08	
		Ours	✓		71.10	45.91	59.82	32.00	52.21	
		Ours	✓	✓	72.36	45.91	58.64	32.25	52.29	
	3-4-16	BitDistiller			73.34	50.94	63.61	34.81	55.68	
		Ours	✓		76.71	53.96	68.19	35.23	58.52	
		Ours	✓	✓	77.20	53.11	68.43	38.82	59.39	
	3-4-4	BitDistiller			73.06	50.78	65.03	35.32	56.05	
		Ours	✓		76.98	53.12	66.77	37.03	58.48	
		Ours	✓	✓	75.46	53.06	67.88	37.80	58.55	
	2-7B	16-16-16				77.86	57.14	68.35	43.34	61.67
		2-4-16	BitDistiller			62.95	37.33	50.20	22.95	43.36
Ours			✓		70.13	45.02	60.77	30.03	51.49	
Ours			✓	✓	69.48	45.22	59.75	29.95	51.10	
2-4-4		BitDistiller			62.70	37.18	53.91	25.93	44.93	
		Ours	✓		69.53	45.67	59.35	29.86	51.10	
		Ours	✓	✓	69.91	44.58	59.70	30.69	51.22	
3-4-16		BitDistiller			74.42	51.36	62.66	36.17	56.15	
		Ours	✓		76.06	54.26	66.45	40.35	59.28	
		Ours	✓	✓	76.65	54.25	67.80	40.35	59.74	
3-4-4		BitDistiller			72.41	50.51	63.29	35.83	55.51	
		Ours	✓		76.55	53.55	65.90	39.33	58.83	
		Ours	✓	✓	76.71	53.88	65.43	41.04	59.27	
3-8B		16-16-16				80.70	79.60	73.70	57.70	72.93
		2-4-16	BitDistiller			57.23	29.96	49.48	21.16	39.46
	Ours		✓		69.96	44.30	59.43	28.66	50.59	
	Ours		✓	✓	69.16	44.67	59.91	29.69	50.86	
	2-4-4	BitDistiller			56.42	29.57	52.09	20.90	39.75	
		Ours	✓		69.15	43.62	57.85	28.58	49.80	
		Ours	✓	✓	69.97	44.32	59.51	27.82	50.41	
	3-4-16	BitDistiller			72.47	49.72	62.43	36.94	55.39	
		Ours	✓		77.25	55.18	68.90	42.91	61.06	
		Ours	✓	✓	77.64	55.21	69.93	43.34	61.53	
	3-4-4	BitDistiller			73.32	49.97	64.87	37.45	56.35	
		Ours	✓		75.35	53.95	67.64	41.80	59.69	
		Ours	✓	✓	76.16	54.35	71.19	42.75	61.11	

Table 8: Complete comparison of accuracy on Zero-shot Common Sense Reasoning tasks on LLaMA models with parameter sizes of at least 7B.

Model	#Bits (W-A-KV)	Configuration			PIQA	Hella.	Wino.	ARC-c	Avg.	
		Method	Rotation	LDP						
1B	16-16-16				75.30	60.70	60.90	38.70	58.90	
	2-4-16	BitDistiller			51.95	27.41	48.46	19.45	36.82	
		Ours	✓		61.15	30.66	50.67	21.84	41.08	
		Ours	✓	✓	61.42	31.55	51.78	20.65	41.08	
	2-4-4	BitDistiller			55.33	26.62	48.46	19.79	37.55	
		Ours	✓		61.75	30.05	51.22	20.05	40.77	
		Ours	✓	✓	60.71	31.54	53.51	21.42	41.80	
	3-4-16	BitDistiller			53.53	28.35	48.61	19.62	37.53	
		Ours	✓		69.53	40.31	55.40	26.27	47.88	
		Ours	✓	✓	69.64	40.57	56.12	26.37	48.18	
	3-4-4	BitDistiller			54.18	28.26	50.90	21.67	38.75	
		Ours	✓		68.98	37.80	55.40	26.36	47.14	
		Ours	✓	✓	68.12	39.30	56.12	26.11	47.41	
	3B	16-16-16				76.00	71.00	66.60	47.60	65.30
		2-4-16	BitDistiller			54.02	26.80	52.48	18.25	37.89
			Ours	✓		65.99	36.51	52.48	26.19	45.29
			Ours	✓	✓	65.43	37.35	54.70	25.43	45.71
		2-4-4	BitDistiller			51.84	26.70	51.38	19.11	37.26
Ours			✓		64.30	36.26	51.38	25.08	44.26	
Ours			✓	✓	65.45	36.66	53.75	26.37	45.56	
3-4-16		BitDistiller			52.72	26.66	50.43	19.45	37.32	
		Ours	✓		74.04	49.56	63.22	35.83	55.66	
		Ours	✓	✓	73.77	49.52	62.65	37.54	55.87	
3-4-4		BitDistiller			53.91	26.82	48.03	20.30	37.27	
		Ours	✓		74.31	49.19	60.06	36.77	55.08	
		Ours	✓	✓	73.18	48.87	62.43	36.01	55.12	

Table 9: Complete comparison of accuracy on Zero-shot Common Sense Reasoning tasks on LLaMA-3.2 models with parameter sizes of at most 3B.

Layer Size	FP16	RCP	RCP+FP16Had	RCP+FP32Had	QuaRot	QuaRot+FP16Had	QuaRot+FP32Had
(2048, 8192)	0.054	0.036	0.110	0.146	0.073	0.155	0.186
(3072, 8192)	0.054	0.035	0.169	0.198	0.074	0.212	0.237
(4096, 11008)	0.077	0.048	0.120	0.148	0.088	0.157	0.186
(4096, 14336)	0.110	0.059	0.121	0.149	0.079	0.157	0.183

Table 10: GEMV latency for the down projection is measured except activation quantization overhead. The layer size is composed as (input channel, output channel). All latency numbers are in milliseconds.

Layer Size	RCP	RCP+FP16Had	RCP+FP32Had	QuaRot	QuaRot+FP16Had	QuaRot+FP32Had
(2048, 2048)	0.131	0.214	0.248	0.170	0.248	0.276
(3072, 3072)	0.131	0.265	0.295	0.168	0.304	0.331
(4096, 4096)	0.133	0.221	0.250	0.174	0.250	0.282

Table 11: GEMV latency for the value projection is measured including activation quantization overhead. The layer size is composed as (input channel, output channel). All latency numbers are in milliseconds.

Layer Size	RCP	RCP+FP16Had	RCP+FP32Had	QuaRot	QuaRot+FP16Had	QuaRot+FP32Had
(2048, 8192)	0.143	0.218	0.240	0.186	0.261	0.289
(3072, 8192)	0.140	0.271	0.294	0.177	0.318	0.340
(4096, 11008)	0.143	0.223	0.250	0.177	0.264	0.288
(4096, 14336)	0.142	0.226	0.247	0.177	0.259	0.285

Table 12: GEMV latency for the down projection is measured including activation quantization overhead. The layer size is composed as (input channel, output channel). All latency numbers are in milliseconds.

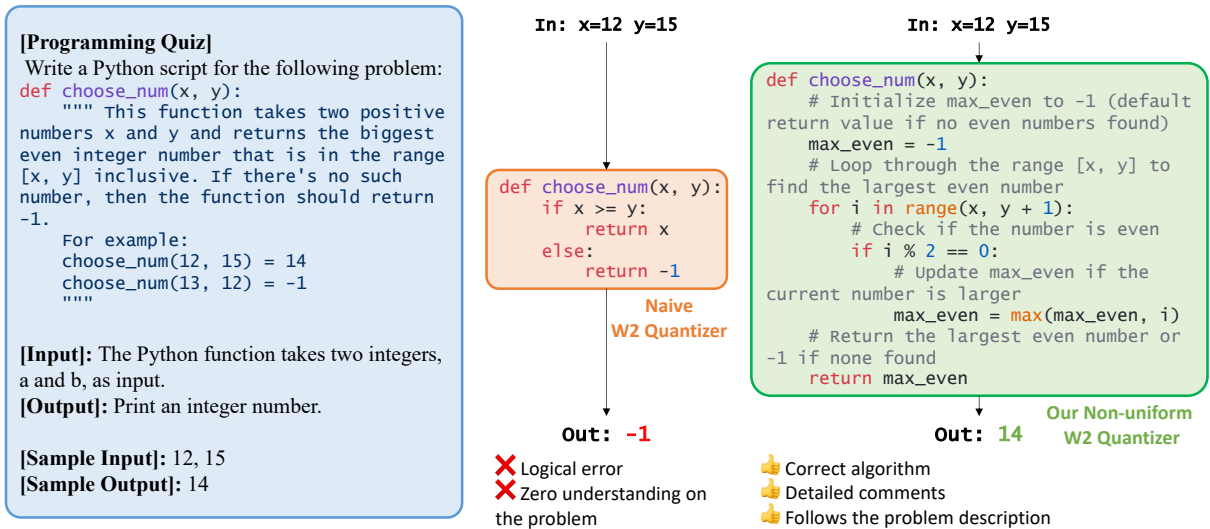


Figure 8: A reasoning task example from HumanEval (Chen et al., 2021) benchmark, conducted by two differently quantized WizardCoder-7B (Luo et al., 2023) models. The results in the orange box is from state-of-the-art QAT method BitDistiller (Du et al., 2024) with applying rotation. In the green box, our proposed RCP is applied. Both methods employ exactly the same 4-bit quantization setting for activation and KV-cache.